ON-ORBIT CROSS CALIBRATION BETWEEN THE OSIRIS-REX ORBITING LASER ALTIMETER AND NAVIGATION CAMERA

Andrew J. Liounis[1*], Jason M. Leonard[2], Kenneth Getzandanner[1], Brent J. Bos[1], and Michael G. Daly[3]; [1]Goddard Space Flight Center (8800 Greenbelt Rd, Greenbelt, MD 20771) [2]KinetX Inc. (21 W Easy St. No. 108, Simi Valley, CA 93065) [3]Centre for Research in Earth and Space Science (CRESS) 416 Petrie Science and Engineering Building, York University, 4700 Keele Str, Toronto, ON M3J 1P3 [*][andrew.j.liounis@nasa.gov]

Abstract. *Accurate shape models of small bodies provide both science value and resources for precision relative navigation. One instrument commonly used for generating shape models is the laser altimeter. Laser altimeters require accurate intrinsic and extrinsic calibration knowledge to produce accurate shape models. Here, we describe a method used for updating the intrinsic and extrinsic calibration parameters of the laser altimeter onboard the Origins, Spectral Interpretation, Resource Identification, and Security–Regolith Explorer (OSIRIS-REx) spacecraft, OLA (OSIRIS-REx Laser Altimeter). We perform the calibration update by comparing the OLA scans with monocular camera images of the asteroid surface captured by the primary navigation camera.*

Introduction. The Origins, Spectral Interpretation, Resource Identification, and Security–Regolith Explorer (OSIRIS-REx) mission to the asteroid Bennu successfully collected a sample of Bennu's surface in October of 2020 after having navigated in proximity to Bennu for about 2 years.[1,2] Throughout proximity operations at Bennu, the navigation team utilized relative measurements between the spacecraft and Bennu to achieve very accurate knowledge of the spacecraft's state, down to the sub-meter level.[3–5] The most commonly used relative measurement during this time period was terrain relative navigation (TRN), where known features from Bennu's surface were identified in monocular images of the surface[6,7] captured by the primary navigation camera (NavCam 1).[8,9] An accurate shape model of Bennu's surface was required in order to determine these known surface features used for TRN.

Multiple methods of building the shape model of Bennu were used on the OSIRIS-REx project. The primary method uses a process known as stereophotoclinometry (SPC) to create a detailed shape model from only monocular images of the surface.[10,11] This technique produces excellent shape models for navigation purposes, but can sometimes tend to smooth the terrain from what is actually observed. Therefore, a secondary method to generate a shape model was also used on the project, originally intended purely for science purposes. In this secondary method, global 3D point clouds from scans of Bennu's surface captured by the 2-axis scanning OSIRIS-REx Laser Altimeter (OLA) were aligned and stitched together to create a global 5cm resolution map of Bennu's surface without the flattening effects of SPC.[10,12,13]

In order to ensure that the resulting shape model from the OLA scans was accurate, the intrinsic and extrinsic calibration parameters for OLA needed to be known precisely. In the first attempt to build a shape model in this method, it was discovered that the ground calibration of these parameters was no longer valid, as the resulting shape model had the wrong aspect ratio and areas of high residuals. Therefore, an on-orbit re-calibration of the OLA intrinsic and extrinsic parameters was undertaken by the project. The official method for doing this, resulting in the published parameters, involved calibrating OLA by comparing overlapping scans of the same surface region as described in Ref. 14.

Additional on-orbit calibration methods were also developed by the navigation team for OSIRIS-REx while investigating the overall scale of Bennu, including cross-calibration with NavCam 1, calibration through the use of overlapping OLA scans, calibration in the larger orbit determination and geodesy framework,[15] and cross-validation with the guidance navigation and control (GNC) laser imaging, detection, and ranging (LiDAR) sensor.[16] In the NavCam 1 cross-calibration method, the focus of this paper, the OLA scans are compared against monocular images captured by NavCam 1 during the scan. This provides the opportunity to not only calibrate the OLA intrinsic parameters against the NavCam 1 images, but also the relative extrinsic parameters (position and orientation) between OLA and NavCam 1, which is another important parameter for the precision navigation. In the rest of this paper, we describe the steps taken to perform this calibration and then present the results from using it on the flight OLA and NavCam 1 data. We also discuss the limitations of the approach and briefly compare it to the results using the official calibration procedure undertaken by the project.

Methodology. To perform the cross-calibration between OLA and NavCam 1, we used similar techniques to TRN, where we render the individual OLA scans (after tessellating them) and then use cross-correlation to match the images with the scans. This then gives us correspondences between the OLA scans and the images, which can be put into a large linearized-least squares estimator to estimate the calibration parameters. A detailed process for generating the measurements feeding into the batch least squares follows.

1. Identify OLA scans where a NavCam 1 image was captured during the scan.

2. Create the body-fixed location for each OLA return using the current estimate of the calibration and the

spacecraft position knowledge.

3. Tessellate the body-fixed locations from a single scan to create the observed surface.

4. Using the current estimates of the spacecraft position and attitude, render the OLA scan surfaces into the image space using a single bounce ray tracer.

5. Split the rendered scans into tiles of about 100x100 pixels.

6. For each tile from the rendered scans, use normalized cross-correlation to align the tile to the captured images. The measurements then are the shifts from the expected tile location in the image to the observed tile location in the image.

An example of the residuals resulting from this process for a single scan/image pair is shown in Fig. 1.

Once the measurements have been extracted for each scan-image pair, the linearized-least squares estimation can be performed. Specifically, in the estimation process we determine the following parameters:

- A scaling multiplier for each axis of the scanning mirror position.
- A range bias parameter for each mode of the altimeter (high energy mode and low energy mode).
- A relative attitude correction between OLA and NavCam 1 for each image/scan pair.
- Optionally, a 3-axis shift between OLA and NavCam 1 in the spacecraft-fixed frame for all image/scan pairs.

We use an inner/outer least squares loop, where we first minimize the residuals without recreating the OLA point clouds and template, and then we take the results from the inner optimization to recompute the OLA point clouds and template. All of these steps are performed making use of existing capabilities from the Goddard Image Analysis and Navigation Tool (GIANT).[17]

We now provide more details on each of the preceding steps in the following subsections.

Identify OLA–NavCam 1 Overlaps. The first step in the cross-calibration is to identify periods in the orbit where a NavCam 1 image was captured simultaneously while an OLA scan was also being captured. We restrict ourselves to simultaneous for two reasons. First, this ensures that the OLA scan pattern will fall within the NavCam 1 field of view. Second, this minimizes the effects of navigational errors in the calibration, which grow with the separation time between the image and scan. Specifically, this reduces the dependence on the estimated spacecraft trajectory to be primarily the in-track velocity (since we rely directly on the OLA return values for range, not the spacecraft trajectory).

Create Point Cloud From OLA Scan Data. Next, for each OLA scan identified, we convert the OLA range returns into 3D point clouds expressed in the Bennu-centered, Bennu-fixed frame. This requires using the current estimate of the OLA intrinsic parameters (scan mirror scales and range biases), the OLA extrinsic parameters (OLA frame alignment with the spacecraft frame, OLA offset from the spacecraft COM), and the estimate of the spacecraft's position in the Bennu-centered, Bennu-fixed frame. Though this step has a dependency on the spacecraft navigation state, the dependence is minimized because the same state is used with the NavCam 1 data (hence the requirement for simultaneous overlap), thus the effective dependency is only on the velocity of the spacecraft and only for the duration of the OLA scan.

Tessellate the OLA Point Cloud. We now take the OLA point cloud from each scan, and tessellate it into a triangular meshed continuous surface. This allows us to treat the point clouds as surfaces in GIANT and render what we expect the surface should look like. There are a number of ways to perform this tessellation, but in our analysis we convert each 3D point into a latitude/longitude location in the Bennu-fixed frame, then use a 2D Delaunay triangulation.[18–20] The result is a set of vertices in the Bennu-centered, Bennu-fixed frame (the OLA point cloud) along with a connectivity matrix, which are then converted into a GIANT triangle surface.

Render the OLA Templates. With the OLA data now converted into a surface, we can render this surface into the NavCam 1 image frame using the estimated spacecraft state at the time of the image, Bennu's spin state at the time of the image, the NavCam 1 inertial pointing at the time of the image (estimated from an image of a star field),[7] and the NavCam 1 intrinsic calibration (estimated from images of star fields).[9] We first transform the surface from the Bennu-centered, Bennu-fixed frame into the NavCam 1 frame, correcting for light time and stellar aberration. We then perform a single-bounce ray trace from NavCam 1, to the surface, and then to the sun to determine the intersect locations, the surface normal at each intersect location, and whether each intersect was shadowed by some other piece of the OLA surface, or illuminated. We then take this data and feed it into the McEwen reflectance function[21] to determine the predicted intensity for each pixel being rendered. This provides a 2D template of what we think the OLA scan should look like in the NavCam 1 image based on all of the current estimates.

Split the OLA Templates. With the full templates of the OLA scans rendered in the NavCam 1 image, we now split the templates into approximately 100x100 pixel grids, chosen to closely resemble the size of templates used in traditional surface feature navigation (SFN) analysis. These grids enable us to extract multiple measurements from each OLA scan-NavCam 1 image overlap across the entire OLA scan. This is important because the OLA intrinsic parameters will cause distortions in the rendered

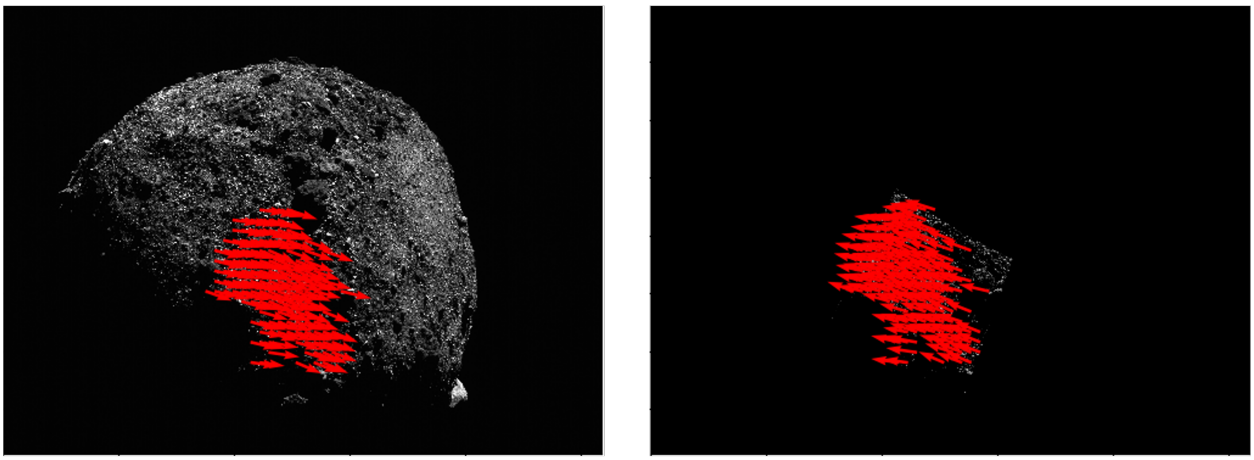

Figure 1. An example of the residuals observed from a single scan-image pair using the discussed technique. Both the image (left) and rendered scan (right) are shown.

template as they are changed, rather than global shifts. With multiple points from each scan, we can begin to observe these distortions in our estimation process.

Extract the OLA-NavCam Measurements. With the split OLA templates, we can now extract our measurements from the OLA scan-NavCam 1 image pairs. For each tile in each template, we find the best alignment to the corresponding NavCam 1 image using normalized cross correlation, as is typical for OpNav techniques like SFN.[22] The result from the correlation based alignment is a shift between the predicted tile location (the original center of the tile in the image) and the observed tile location (the location of the center of the tile in the image which produces the highest correlation score). These shifts are the observed minus computed residuals we feed into the linearized least squares process.

Linearized Least Squares. We can now minimize our observed minus computed residuals in a least squares sense. As mentioned previously, we do this in an inner/outer loop design.

Inner Loop. In the inner loop, we do not recreate the OLA Scan tiles at each step, instead focusing on optimizing the computed location of each tile by updating the OLA intrinsic and extrinsic parameters, along with an attitude correction for each OLA scan. Changing these parameters changes how the center of the each OLA tile projects into the NavCam 1 images in much the same way that adjusting the spacecraft position and pointing knowledge changes how surface feature locations project into images when solving the perspective-n-points (PnP) problem as is done in SFN.[22] The attitude correction is important to remove any large initial errors in the residuals which could mask the effects of the intrinsic parameters. Because this is linearized least squares, we linearize the non-linear measurement model by taking the partial derivative of the measurement model with respect to the various parameters being estimated in the typical fashion. We also therefore must iteratively minimize the residuals until convergence. The derivation of the analytical partial derivatives is particular to the parameters being estimated as well as the models of the instruments being considered and is therefore left to the reader.

Outer Loop. In the outer loop, we take the current estimate of the various parameters from the last inner loop iteration and use it to recompute the OLA tile measurements (the observed locations). This involves repeating steps 2–6 from before. Once we have regenerated the observed locations, we re-enter into the inner loop. The looping continues until convergence criteria are met.

Results. We now provide a brief discussion of the results using this technique to validate the intrinsic calibration of the OLA instrument. The OLA instrument is unique in that it is a scanning altimeter and additionally carries 2 different powered modes. This leads to the intrinsic parameters of the OLA model being the azimuth scan mirror scaling (α), the elevation scan mirror scaling (β), an additive range bias for the high energy laser mode (b_h), and an additive range bias for the low energy laser mode (b_l). For this analysis, we identified 69 instances when a NavCam 1 image was captured during an OLA scan, of which we chose 30 to fit within computational resources. These parings produced about 1600 observables (after removing outliers) that could be used to estimate the calibration of OLA.

Observability Analysis. To begin, we simply looked at the formal covariance matrix for all of the intrinsic and extrinsic parameters to identify which were observable for our anlysis, shown in Fig. 2. As shown in the figure, the uncertainty on the range biases is very high (on the order of 1.25 meters 1σ), indicating that the range bias is largely unobservable (since it is expected to be on the 20cm level).[15] Additionally, there is high correlation between the shift in the spacecraft frame (p_x, p_y, and p_z) and a number of the parameters, including the scan mirror scale parameters (α and β) and the sample frame correction (r_x, r_y, and r_z). Based on this, we determined

that the range biases and the shift in the spacecraft frame are largely unobservable from this dataset (which makes intuitive sense given that monocular images are not particularly sensitive to changes in distance or small lateral shifts). Therefore, we only chose to estimate the scan mirror scales (α and β) and the frame offsets ($r_x - r_z$ per image-scan pair).

Estimation Performance. We then turned to performing the actual calibration using the methods discussed in this paper. We set the *a priori* values for the mirror scales to 1 for each axis, the range bias for the high energy and low energy laser to 20 cm and 0 cm,[15] respectively (since we were not estimating these), the initial frame offset for each pair to 0 radians each axis, and the positional shift between OLA and NavCam 1 in the spacecraft frame to 0 cm. This resulted in an estimate of 1.007133 for the azimuth mirror scaling, 0.9994 for the elevation mirror scaling, and frame corrections around 0.1 degrees per each scan-image pairing. All of these estimates have high signal-to-noise ratios, indicating that the estimator is confident in the values. The official scan mirror estimates from other approaches are 1.0073 and 1.0, respectively (elevation scaling was fixed at 1.0),[14] showing that the technique was able to achieve good agreement within the bounds of the formal uncertainty (within 1 sigma). The modified covariance matrix from this calibration is shown in Fig. 3. The *a priori* residuals before the calibration are shown in Fig. 4. The post-fit residuals after the calibration are shown in Fig. 5. As can be seen, the calibration process greatly reduces the residuals to within the expected performance bounds. In the post-fit residuals, we believe that the bi-modal distribution in the x-direction is due to a poor image-scan frame alignment estimate for a single pair, likely caused by a small collection of outliers.

Conclusion. In this paper, we described a novel cross calibration technique between a 3D scanning laser altimeter and a monocular 2D camera which involves rendering the scans of the altimeter into the image and using least squares to estimate the intrinsic and extrinsic parameters which control the scan point cloud and projection. The technique was shown to work for the OSIRIS-REx OLA and NavCam 1 instruments, producing results that agree well with the official calibration from the project. However, just as other techniques have shown, this technique is also unable to fully resolve the intrinsic parameters of OLA (specifically, the range biases are largely unobservable). This technique provides a unique concept for future in-flight cross-calibration of altimeters, LiDARs, and monocular cameras. Though in this paper we focused primarily on estimating the intrinsic parameters for the altimeter, this process should be equally valid for estimating the intrinsic characteristics of the monocular camera as well with a different set of partial derivatives.

References.

[1] D. Lauretta, S. Balram-Knutson, E. Beshore, W. Boynton, C. Drouet d'Aubigny, D. DellaGiustina, H. Enos, D. Golish, C. Hergenrother, E. Howell, *et al.*, "OSIRIS-REx: Sample Return from Asteroid (101955) Bennu," *Space Science Reviews*, vol. 212, no. 1, pp. 925–984, 2017.

[2] D. S. Lauretta, H. L. Enos, A. T. Polit, H. L. Roper, and C. W. Wolner, "OSIRIS-REx at Bennu: Overcoming challenges to collect a sample of the early Solar System," in *Sample return missions*, pp. 163–194, Elsevier, 2021.

[3] P. G. Antreasian, C. D. Adam, K. Berry, J. Geeraert, K. M. Getzandanner, D. Highsmith, J. M. Leonard, E. J. Lessac-Chenen, A. H. Levine, J. V. McAdams, L. K. McCarthy, M. C. Moreau, D. Nelson, B. Page, J. Pelgrift, S. M. Rieger, E. Sahr, D. Wibben, B. G. Williams, K. Williams, and D. Lauretta, "OSIRIS-REx Proximity Operations and Navigation Performance at Bennu," in *AIAA SCITECH 2022 Forum*.

[4] J. M. Leonard, J. L. Geeraert, B. R. Page, A. S. French, P. G. Antreasian, C. D. Adam, D. R. Wibben, M. C. Moreau, and D. S. Lauretta, "OSIRIS-REx Orbit Determination Performance During the Navigation Campaign," in *2019 AAS/AIAA Astrodynamics Specialist Conference*, no. AAS 19-714, 2019.

[5] J. M. Leonard, J. Geeraert, J. Pelgrift, P. G. Antreasian, C. D. Adam, D. Wibben, K. M. Getzandanner, B. W. Ashman, and D. Lauretta, "Navigation Prediction Performance During the OSIRIS-REx Proximity Operations at (101955) Bennu," in *AIAA SCITECH 2022 Forum*.

[6] B. Williams, P. Antreasian, E. Carranza, C. Jackman, J. Leonard, D. Nelson, B. Page, D. Stanbridge, D. Wibben, K. Williams, *et al.*, "OSIRIS-REx Flight Dynamics and Navigation Design," *Space Science Reviews*, vol. 214, no. 4, pp. 1–43, 2018.

[7] C. D. Adam, S. Knutson, O. Billett, M. C. Moreau, P. G. Antreasian, B. J. Bos, A. Calloway, N. Castro, J. Cavaluzzi, B. T. Carcich, *et al.*, "Concept of Operations for OSIRIS-REx Optical Navigation Image Planning," in *AIAA SCITECH 2022 Forum*, p. 1569, 2022.

[8] B. Bos, M. Ravine, M. Caplinger, J. Schaffner, J. Ladewig, R. Olds, C. Norman, D. Huish, M. Hughes, S. Anderson, *et al.*, "Touch And Go Camera System (TAGCAMS) for the OSIRIS-REx Asteroid Sample Return Mission," *Space Science Reviews*, vol. 214, no. 1, pp. 1–23, 2018.

[9] B. Bos, D. Nelson, J. Pelgrift, A. Liounis, D. Doelling, C. Norman, R. Olds, C. May, R. Witherspoon, E. Church, *et al.*, "In-flight Calibration and Performance of the OSIRIS-REx Touch and Go Camera System (TAGCAMS)," *Space Science Reviews*, vol. 216, no. 4, pp. 1–52, 2020.

[10] O. Barnouin, M. Daly, E. Palmer, C. Johnson, R. Gaskell, M. Al Asad, E. Bierhaus, K. Craft, C. Ernst, R. Espiritu, *et al.*, "Digital Terrain Mapping by the OSIRIS-REx Mission," *Planetary and Space Science*, vol. 180, p. 104764, 2020.

[11] O. Barnouin, M. Daly, E. Palmer, R. Gaskell, J. Weirich, C. Johnson, M. Al Asad, J. Roberts, M. Perry, H. Susorney, *et al.*, "Shape of (101955) Bennu Indicative of a Rubble Pile with Internal Stiffness," *Nature geoscience*, vol. 12, no. 4, pp. 247–252, 2019.

[12] M. Daly, O. Barnouin, C. Dickinson, J. Seabrook, C. Johnson, G. Cunningham, T. Haltigin, D. Gaudreau, C. Brunet, I. Aslam, *et al.*, "The OSIRIS-REx Laser Altimeter (OLA) Investigation and Instrument," *Space Science Reviews*, vol. 212, no. 1, pp. 899–924, 2017.

[13] J. Seabrook, M. Daly, O. Barnouin, C. Johnson, A. Nair, E. Bierhaus, W. Boynton, R. Espiritu, R. Gaskell, E. Palmer, *et al.*, "Global Shape Modeling Using the

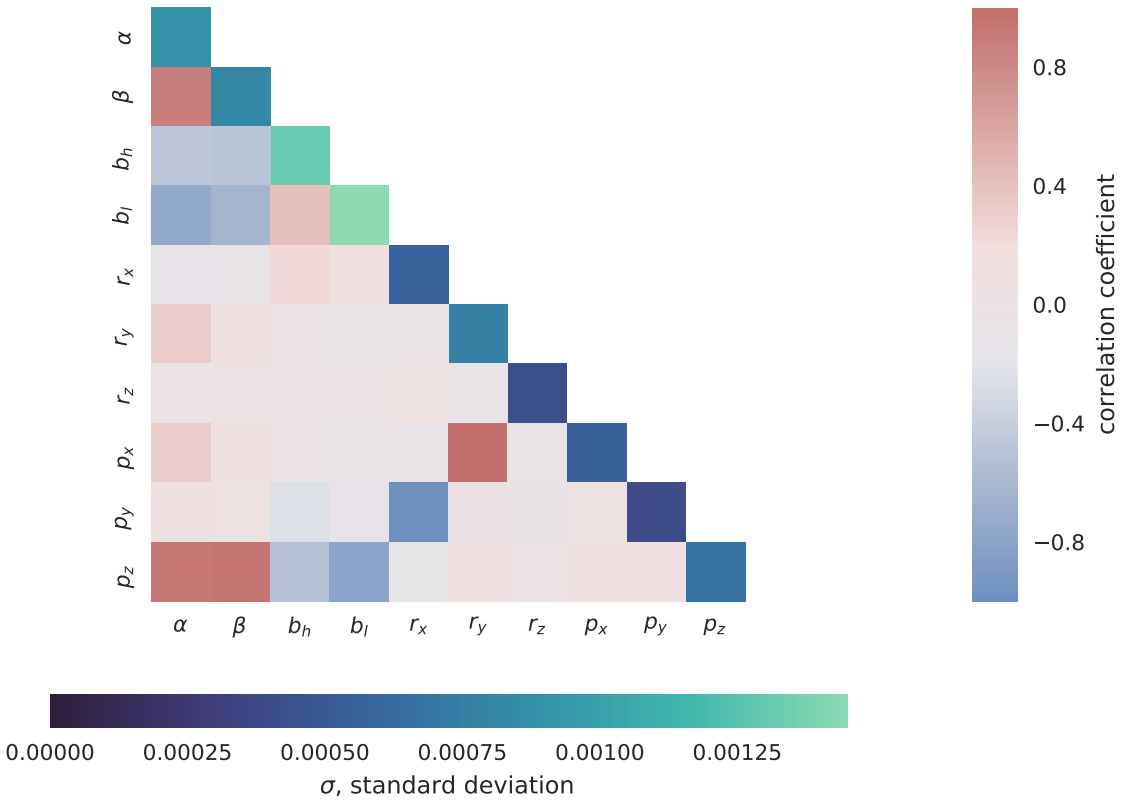

Figure 2. The modified covariance matrix shown as a double heatmap assuming measurement uncertainty of 1 pixel 1σ***. The main diagonal represents the*** 1σ ***uncertainty for each parameter and utilizes the horizontal colormap depicted along the bottom of the figure. The off-diagonal elements depict the correlation coefficient (between -1 and 1, with 1 implying perfect correlation) and utilize the vertical colormap depicted along the right of the figure. The parameters are:*** α ***is the scaling of the azimuth mirror angle,*** β ***is the scaling of the elevation mirror angle,*** b_h ***is the range bias for the high energy laser in units of km,*** b_l ***is the range bias for the low energy laser in units of km,*** r_{x-z} ***is an example of the frame offset between OLA and NavCam 1 (repeated for each scan-image pairing) represented as a rotation vector, and*** p_{x-z} ***is the shift in the spacecraft-fixed frame in units of km.***

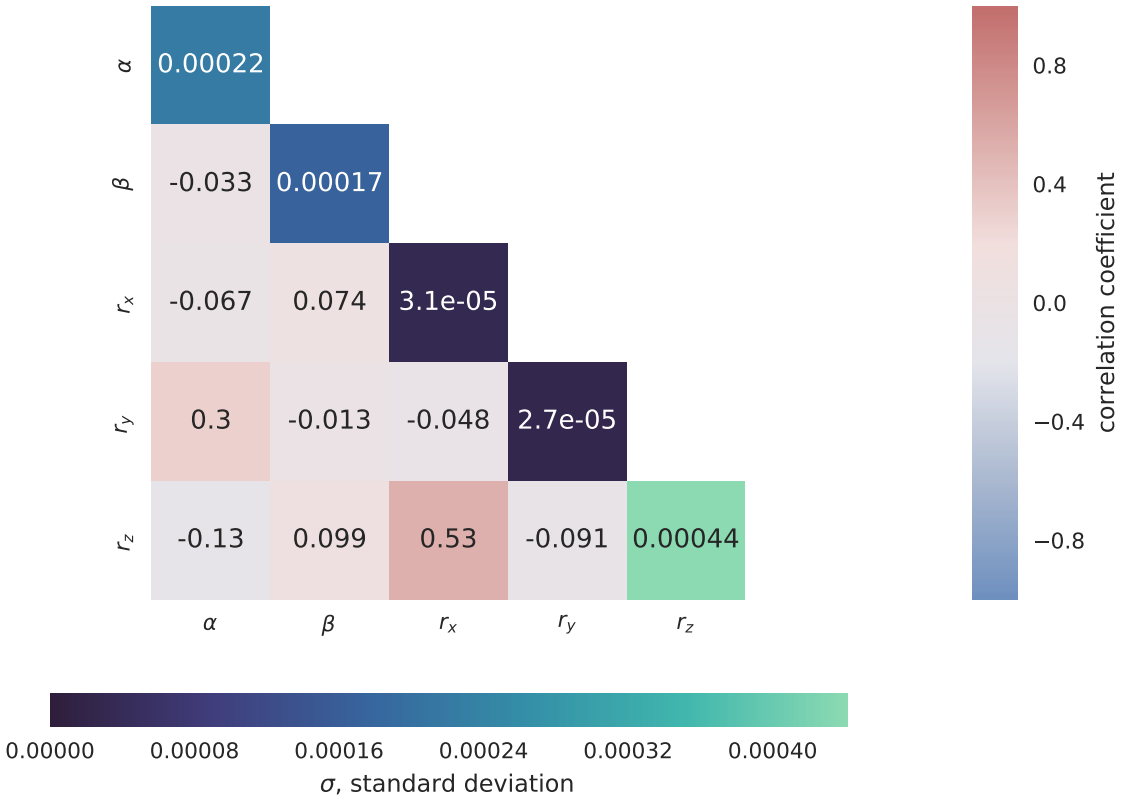

Figure 3. The modified covariance matrix shown as a double heatmap assuming measurement uncertainty of 1 pixel 1σ***. The main diagonal represents the*** 1σ ***uncertainty for each parameter and utilizes the horizontal colormap depicted along the bottom of the figure. The off-diagonal elements depict the correlation coefficient (between -1 and 1, with 1 implying perfect correlation) and utilize the vertical colormap depicted along the right of the figure. The parameters are:*** α ***is the scaling of the azimuth mirror angle,*** β ***is the scaling of the elevation mirror angle, and*** r_{x-z} ***is an example of the frame offset between OLA and NavCam 1 (repeated for each scan-image pairing) represented as a rotation vector.***

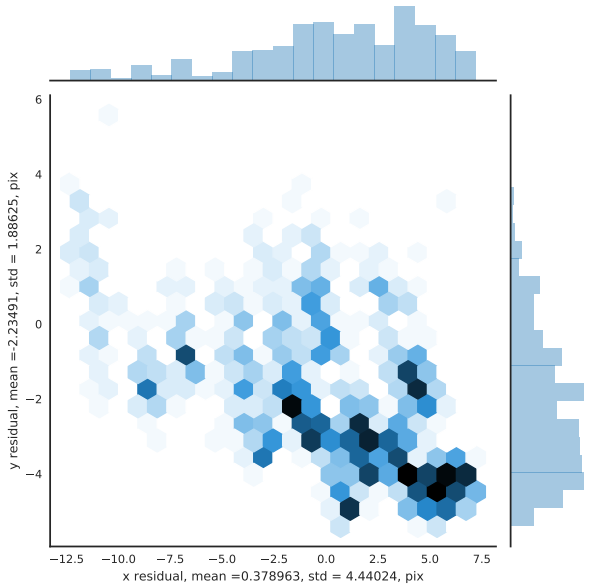

Figure 4. The a priori residuals in the image shown as a hexbin plot (darker colors indicate more points in the bin). The distribution is shown along the upper and right axes, respectively, as histograms.

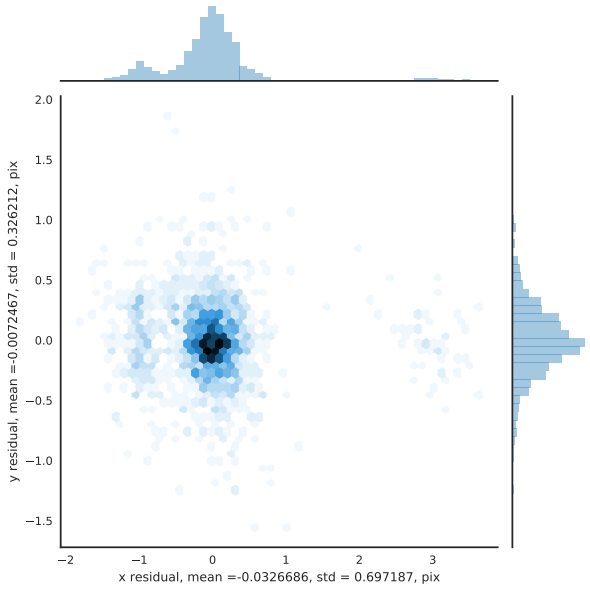

Figure 5. The post-fit residuals in the image shown as a hexbin plot (darker colors indicate more points in the bin). The distribution is shown along the upper and right axes, respectively, as histograms. The residuals are much more Gaussian and not biased with the exception of some possible outliers.

OSIRIS-REx Scanning Laser Altimeter," *Planetary and Space Science*, vol. 177, p. 104688, 2019.

[14] J. A. Seabrook, M. G. Daly, O. S. Barnouin, E. E. Palmer, R. Gaskell, H. Nair, and D. S. Lauretta, "Building a High-Resolution Digital Terrain Model of Bennu from Laser Altimetry Data," *Planetary Science Journal*, submitted: 2022.

[15] S. Goossens, D. D. Rowlands, E. Mazarico, A. J. Liounis, J. L. Small, D. E. Highsmith, J. C. Swenson, J. R. Lyzhoft, B. W. Ashman, K. M. Getzandanner, J. M. Leonard, J. L. Geeraert, C. D. Adam, P. G. Antreasian, O. S. Barnouin, M. G. Daly, J. A. Seabrook, and D. S. Lauretta, "Mass and shape determination of (101955) bennu using differenced data from multiple OSIRIS-REx mission phases," *The Planetary Science Journal*, vol. 2, p. 219, nov 2021.

[16] J. M. Leonard, M. C. Moreau, P. G. Antreasian, K. M. Getzandanner, E. Church, C. Miller, M. G. Daly, O. S. Barnouin, and D. S. Lauretta, "Cross-Calibration of GNC and OLA LiDAR Systems Onboard OSIRIS-REx," no. AAS 22-166, 2022.

[17] A. J. Liounis, C. Gnam, J. Swenson, K. Getzandanner, J. Small, and J. Lyzhoft, "The Goddard Image Analysis and Navigation Tool," 1 2022. https://github.com/nasa/giant.

[18] B. Delaunay *et al.*, "Sur la sphere vide," *Izv. Akad. Nauk SSSR, Otdelenie Matematicheskii i Estestvennyka Nauk*, vol. 7, no. 793-800, pp. 1–2, 1934.

[19] C. B. Barber, D. P. Dobkin, and H. Huhdanpaa, "The quickhull algorithm for convex hulls," *ACM TRANSACTIONS ON MATHEMATICAL SOFTWARE*, vol. 22, no. 4, pp. 469–483, 1996.

[20] P. Virtanen, R. Gommers, T. E. Oliphant, M. Haberland, T. Reddy, D. Cournapeau, E. Burovski, P. Peterson, W. Weckesser, J. Bright, S. J. van der Walt, M. Brett, J. Wilson, K. J. Millman, N. Mayorov, A. R. J. Nelson, E. Jones, R. Kern, E. Larson, C. J. Carey, İ. Polat, Y. Feng, E. W. Moore, J. VanderPlas, D. Laxalde, J. Perktold, R. Cimrman, I. Henriksen, E. A. Quintero, C. R. Harris, A. M. Archibald, A. H. Ribeiro, F. Pedregosa, P. van Mulbregt, and SciPy 1.0 Contributors, "SciPy 1.0: Fundamental Algorithms for Scientific Computing in Python," *Nature Methods*, vol. 17, pp. 261–272, 2020.

[21] A. S. McEwen, "Photometric functions for photoclinometry and other applications," *Icarus*, vol. 92, no. 2, pp. 298–311, 1991.

[22] C. Gnam, A. Liounis, B. Ashman, K. Getzandanner, J. Lyzhoft, J. Small, D. Highsmith, C. Adam, J. Leonard, P. Antreasian, *et al.*, "A Novel Surface Feature Navigation Algorithm Using Ray Tracing," in *2nd RPI Space Imaging Workshop*, 2019.